Nanoscale

Accepted Manuscript

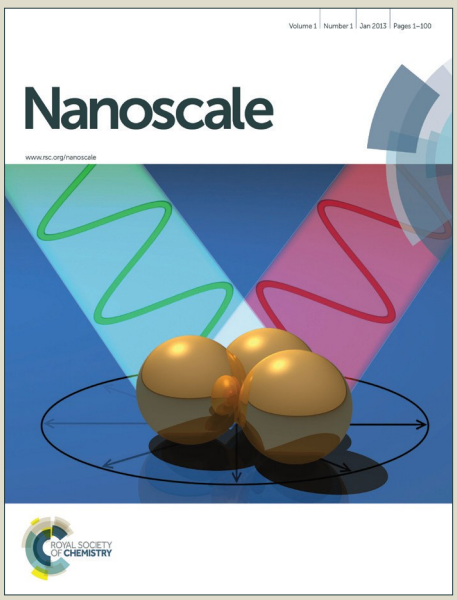

ROYAL SOCIETY OF CHEMISTRY

www.rsc.org/nanoscale

Journal Name

ARTICLE TYPE

Cite this: DOI: 10.1039/xxxxxxxxxx

Topologically protected Dirac plasmons and their evolution across the Quantum Phase Transition in $(Bi_{1-x}In_x)_2Se_3$ Topological Insulator†

Marta Autore,[a] Favio Giorgianni,[a] Fausto D' Apuzzo,[b] Alessandra Di Gaspare,[c] Irene Lo Vecchio,[d] Matthew Brahlek,[e] Nikesh Koirala,[e] Seongshik Oh,[e] Urlich Schade,[f] Michele Ortolani,[c] and Stefano Lupi*[a]

Received Date
Accepted Date

DOI: 10.1039/xxxxxxxxxx

www.rsc.org/journalname

A 3D Topological Insulator (TI), is an intrinsically stratified electronic material characterized by an insulating bulk and Dirac free electrons at the interface with vacuum or another dielectric. In this paper we investigate, through terahertz (THz) spectroscopy, the plasmon excitation of Dirac electrons on thin films of $(Bi_{1-x}In_x)_2Se_3$ TI patterned in form of a micro-ribbon array, across a Quantum Phase Transition (QPT) from the topological to a trivial insulating phase. This latter is achieved by In doping onto the Bi-site and is characterized by massive electrons at the surface. While the plasmon frequency is nearly independent of In content, the plasmon width undergoes a sudden broadening across the QPT, perfectly mirroring the single particle (free electron) behavior as measured on the same films. This strongly suggests that the topological protection from backscattering characterizing Dirac electrons in the topological phase extends also to their plasmon excitations.

Topological insulators are a novel class of quantum materials which show an insulating gap in the bulk and exotic conducting states at the interface with vacuum or another dielectric[1–3]. These states are characterized by a Dirac energy-momentum dispersion ($E \propto p$), spin locked to momentum and backscattering protection in the presence of non-magnetic impurities. The key factor determining the intrinsically stratified electronic structure in TIs is a strong spin-orbit coupling, causing a band inversion and leading to non trivial topological invariants belonging to the Z_2 class[4,5]. The 2-Dimensional (2D) Dirac surface states (DSSs) in topological insulators have attracted a lot of interest because of their potential applications in the fields of spintronics, quantum computing, terahertz (THz) detectors and plasmonics[6–10].

Surface plasmons are collective charge excitations lying onto the surface of metals or doped semiconductors. They are at the basis of plasmonic devices for subwavelength optics, light confinement, sensing and many other applications[11–15]. Dirac plasmonics, *i.e.* plasmonics based on Dirac electrons, shows promising advantages over conventional plasmonic materials like gold, such as high frequency tunability via electrostatic gating, high electric field confinement and strong light-matter coupling[16,17]. Graphene has been the first discovered Dirac material and graphene-based plasmonic devices have been largely studied in recent years, with different patterning structures (ribbon[18], disc, ring arrays[19]), electrostatic gating, and under the effect of magnetic fields[19–21]. Dirac surface states in topological insulators show an additional peculiar feature compared to Dirac carriers in graphene: the spin-momentum locking mechanism implies the presence of a transverse spin wave when a collective charge oscillation is excited[22] and *viceversa*. Moreover, because of time reversal symmetry, DSSs are intrinsically protected from backscattering in absence of magnetic impurities, and this topological protection reflects in reduced transport losses and plasmon robustness even at room temperature[6], in contrast with other 2D electron systems[23].

Recently, the topological protection of DSSs has been studied in

[a] *INFN and Dipartimento di Fisica, Università di Roma "La Sapienza", Piazzale A. Moro 2, I-00185 Roma, Italy.*
[b] *Istituto Italiano di Tecnologia and Dipartimento di Fisica, Università di Roma "La Sapienza", Piazzale A. Moro 2, I-00185 Roma, Italy.*
[c] *CNR - Institute for Photonics and Nanotechnologies, Via Cineto Romano 42, 00156 Rome, Italy.*
[d] *Dipartimento di Fisica, Università di Roma "La Sapienza", Piazzale A. Moro 2, I-00185 Roma, Italy.*
[e] *Department of Physics and Astronomy Rutgers, The State University of New Jersey 136 Frelinghuysen Road Piscataway, NJ 08854-8019 USA.*
[f] *Helmholtz-Zentrum Berlin für Materialien und Energie GmbH Elektronenspeicherring BESSY II, Albert-Einstein-Strasse 15, D-12489 Berlin, Germany.*
[g] *INFN and Dipartimento di Fisica, Università di Roma "La Sapienza", Piazzale A. Moro 2, I-00185 Roma, Italy. Tel: +39 6 4991 3491; E-mail: stefano.lupi@roma1.infn.it*
† Electronic Supplementary Information (ESI) available: [details of any supplementary information available should be included here]. See DOI: 10.1039/b000000x/

$(Bi_{1-x}In_x)_2Se_3$ thin films across the QPT from a topological to a trivial phase occurring for increasing Indium (In) content. Indium substitution weakens the spin-orbit interaction causing, in the region between $x(In) = 0.03$ and 0.07, the removal of the valence band-conduction band inversion, which creates the Dirac surface states. This removal corresponds to the closing and the re-opening of a band-gap Δ in concomitance with the appearence of a "trivial insulating" phase[24]. Both phases are characterized by a band-gap $\Delta \sim 300$ meV, and an extrinsic conducting layer of massive (Schrödinger) electrons at the surface due to band-bending effects. Their surface density is similar to that of Dirac carriers which appears only in the topological phase due to the band inversion mechanism[24].

Time domain terahertz (THz) spectroscopy measurements investigating the single-particle response, have shown a sudden collapse of the electron lifetime across the QPT, which has been associated with the loss of topological protection[25]. However, the effect of the QPT on the collective plasmon excitations has never been investigated. More specifically, a comparison between the plasmon response of Dirac carriers and massive carriers, in compounds having a similar lattice structure and surface carrier density has not been studied so far. In this paper, we fill this gap by investigating the evolution of plasmonic excitations across the QPT, with a particular focus on the plasmon scattering rate Γ_p behavior. We observe a sudden increase of Γ_p mirroring the behavior of the single particle scattering rate Γ_D. This strongly suggests that the topological protection not only acts on the single-particle Dirac excitations as it has been experimentally observed in Ref.[?], but also extends to their collective modes. This result may provide a viable path towards long quantum coherence time of plasmon states even at room temperatures, if all other plasmon decay channels were carefully controlled.[?]

1 Results and discussion

High quality thin films of $(Bi_{1-x}In_x)_2Se_3$ were grown by molecular beam epitaxy (MBE)[27,28], with a thickness of $t = 60$ Quintuple Layers (1 QL $\simeq$ 1 nm), on 10×10 mm^2 Al_2O_3 substrate. Indium substitution was set to $x = 0$, 0.02, 0.03, 0.06, 0.07, thus crossing the QPT, which occurs in the region between $x = 0.04$ and $x = 0.05$ for a film thickness of 60 QL[25] as those measured in this experiment.

All samples have been patterned through Electron Beam Lithography (EBL) and reactive ion-etching at IFN-CNR in Rome, in the form of micro-ribbon arrays of width $W = 8$ μm and period $2W$. A Scanning Electron Microscopy (SEM) picture of x=0 patterned film is shown in Fig. 1a. Patterning the film into ribbons provides the extra momentum ($q \sim \pi/W$) necessary to observe plasmonic modes at finite frequency in an optical experiment[6]. Transmittance spectra $T(\nu)$ in the THz range collected with respect to the bare substrate, have been measured through Fourier Transform Infrared Spectroscopy, using a Bruker Michelson interferometer coupled with the THz synchrotron source at the BESSY II storage ring. All measurements were performed at a temperature of 10 K.

In Fig.1b we show a sketch of the THz experiment. Extinction coefficients $E(\nu) = 1 - T(\nu)$ at 10 K for the unpatterned films are instead shown in Fig. 1c. The two maxima at 1.85 and 4.0 THz correspond to the α and β bulk phonon-modes, respectively[29]. These phonons are superimposed to a Drude-like contribution, which has been associated, for the pure Bi_2Se_3 film, mainly to Dirac free electrons[30,31] (see also SI). Indeed, massive (extrinsic) electrons are strongly incoherent (see below) and their contribution to the single-particle and plasmon excitations at low-frequency is (at least at low-T) negligible.

Extinction coefficient for a thin film on a transparent substrate can be written in terms of its complex conductance $\tilde{G}(\nu) = G_1(\nu) + iG_2(\nu)$ as[32]:

$$E(\nu) = 1 - \frac{1}{[1 + Z_0 G_1(\nu)/(n+1)]^2 + [Z_0 G_2(\nu)/(n+1)]^2} \qquad (1)$$

where $Z_0 = 377$ Ω is the free-space impedance, n is the refractive index of the substrate ($n = 3.2$ for Al_2O_3 in the THz range).

In order to extract the Drude and phonon parameters of the unpatterned films, we fitted extinction data to Eq. 1, where the THz conductance has been described in terms of a Drude-Lorentz model[31]:

$$\tilde{G}(\nu) = \frac{e^2}{h}\frac{iD}{\nu + i\Gamma_D} + \frac{i\nu t}{4\pi}\sum_{j=\alpha,\beta}\frac{S_j^2}{\nu(\nu + i\Gamma_j) - \nu_j^2} + \frac{i\nu t}{4\pi}(1 - \varepsilon_\infty) \qquad (2)$$

where D is the Drude spectral weigth, which should scale with $n^{1/4}$, n being the surface density of Dirac electrons, Γ_D is the Drude scattering rate, and ν_j, S_j and Γ_j are peak frequency, strength and spectral width for the Lorentzian-shaped $\alpha(\beta)$ phonon. The phonon terms, due to their bulk nature, contribute to the surface conductance proportionally to the film thickness t. Finally, ε_∞=30 is the high-frequency dielectric constant due to screening by the valence electrons, as estimated from single-crystal optical measurements[29]. The resulting fits are shown in Fig.1c (red circles), where both the Drude (blue dashed lines), the α (green lines) and β (purple lines) phonon contributions extracted from the fit are separately shown. As one can see, In substitution tends to broaden the phonon excitations, in particular the α mode.The phonon linewidth increasing is determined by the distribution of lattice vibrational frequencies, due to the alloy broadening effect of In atoms in the Bi sites. More interestingly, the Drude shape does not show an appreciable modification for $x \leq 0.03$, while it starts to be more flat for higher In content, *i.e.* by entering in the trivial insulating phase.

Fig. 1d shows extinction spectra (black solid lines) for the patterned films for light polarization perpendicular to the ribbons (see Fig. 1b for the experimental optical scheme). As one can see, the α phonon is replaced by a double absorption. This two peaks structure is preserved *vs.* x, although the peaks' height decreases and the high frequency absorption broadens for increasing In content. We assign these features to the α phonon and to the plasmon of $(Bi_{1-x}In_x)_2Se_3$, mutually interacting *via* a Fano interference[6]. This produces a renormalization of both the phonon and the plasmon frequency, with a hardening of the mode at higher frequency

and a softening of that at lower frequency, independently of their nature (anti-crossing behavior).

In order to extract the plasmon parameters (central frequency ν_p and scattering rate Γ_p),we fit the extinction coefficient through a Fano model[6,34]:

$$E(\nu) = \frac{(\nu' + q(\nu))^2}{\nu'^2 + 1} \frac{g^2}{1 + (\frac{\nu - \nu_p}{\Gamma_p/2})^2} \quad (3)$$

where g is the plasmon's coupling factor to the radiation, ν' represents a renormalized frequency and q is the so-called Fano parameter. These parameters are given by:

$$\nu' = \frac{\nu - \nu_{ph}}{\Gamma_{ph}(\nu)/2} - \frac{\nu - \nu_p}{\Gamma_p/2} \quad (4)$$

$$q(\nu) = \frac{\nu w/g}{\Gamma_{ph}(\nu)/2} + \frac{\nu - \nu_p}{\Gamma_p/2} \quad (5)$$

where $\Gamma_{ph}(\nu)$ represents the plasmon-coupled phonon linewidth, written as:

$$\Gamma_{ph}(\nu) = \frac{2\pi v^2}{1 + (\frac{\nu - \nu_p}{\Gamma_p/2})^2} \quad (6)$$

here w is the radiation-phonon coupling factor and v quantifies the phonon-plasmon interaction. Following this model, we were able to fit the mixed plasmon-phonon profile to extract the bare line shapes of the two modes, as shown in Fig.1d.

While the α- and β-phonons slightly broaden with increasing In concentration, as in the case of the unpatterned film spectra, the plasmon mode (whose characteristic frequency is nearly constant *vs*. In content, solid blue lines) undergoes a sudden broadening across the topological transition. In order to quantify this phenomenon, we report the extracted Γ_p values in Fig.2 (black squares), where the Drude single particle scattering rate Γ_D (as extracted from the present experiment and literature[25]) is also displayed.

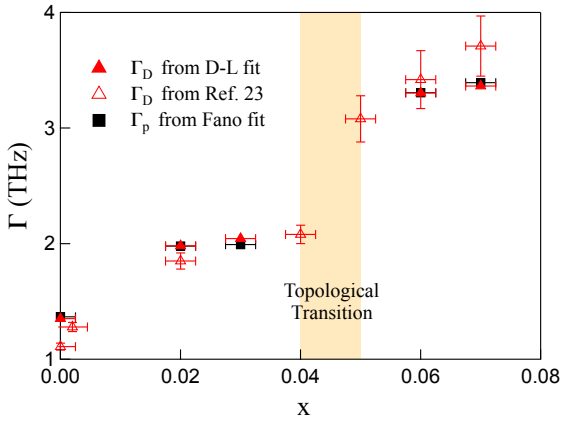

Fig. 2 Comparison between the plasmon scattering rate Γ_p (black squares) and Drude scattering rate Γ_D from the present experiment (red triangles) and literature[25] (red empty triangles), versus In content x at T=10 K. A sudden broadening of both scattering rates can be observed across the QPT transition represented as a shaded yellow region.

As one can clearly see from the Figure 2, the Drude scattering rate Γ_D increases smoothly for low In substitutions ($x \leq 0.04$), which is consistent with the increased impurity scattering. However, around x =0.04 this smooth trend suddenly changes and Γ_D is strongly enhanced. From a pure disorder effect due to In substitution, we would expect a continuous smooth increase of Γ_D. Therefore, the sudden broadening of the Drude term across the QPT strongly indicates the loss of topological protection[28]. This protection, which is associated with the spin-momentum locking mechanism[35], sets to zero the backscattering probability and it is also effective in reducing the scattering effect (and then the dispersion of single-electron momentum) in a wide range of scattering angles between 100°–180°[36].

The plasmon scattering rate Γ_p shows the same steep increase across the QPT (Γ_p passes from 2 THz for x=0.03 to 3.1 THz for x=0.07), perfectly mirroring the single particle scattering rate Γ_D behavior. This represents a strong indication that also Dirac plasmons on TIs surface are topologically protected.

A further insight into the plasmon excitation electrodynamics can be achieved by performing classical electromagnetic simulations for the present plasmonic structure. We can write the polarizability α of a micro-ribbon array in terms of the unpatterned $(Bi_{1-x}In_x)_2Se_3$ complex conductance $\tilde{G}(\nu)$, as[21]

$$\alpha = \frac{W^2}{32/(\varepsilon_1 + \varepsilon_2) - i\nu W/\tilde{G}(\nu)} \quad (7)$$

where W is the ribbon width, while $\varepsilon_1 = n_1^2$ and $\varepsilon_2 = n_2^2$ are the dielectric functions of vacuum and Al_2O_3 substrate, respectively.

As shown in Ref.[21], the transmission coefficient of the patterned structure can be written as

$$t = \frac{2n_1}{n_1 + n_2} \left(1 + \frac{iS}{\alpha^{-1} - D}\right) \quad (8)$$

where $S = (2\pi k_0/2W)[2/(n_1 + n_2)]$, being k_0 the light wavevector, $D = (g/4W^2)[2/(\varepsilon_1 + \varepsilon_2)] + iS$ accounts for the dipole-dipole interaction and, in the long wavelength limit ($\lambda_{light} \gg W$), $g = 2\pi^2/3$. The theoretical extinction coefficient is defined by the following Equation $E = 1 - (|t|^2/|t_0|^2)$, where $t_0 = 2n_1/(n_1 + n_2)$ is the bare substrate transmission coefficient.

Starting from the conductance of the unpatterned films parametrized in terms of the Drude-Lorentz model and using the previous Equations, we were able to calculate for each film and without free parameters the theoretical extinction spectra. These are shown in Fig. 1e (orange empty circles) together with experimental data (black solid lines). It is evident from Fig. 1e that the theoretical calculations well reproduce the overall behavior of the plasmonic structures capturing, in particular, the asymmetric shape of the extinction due to the plasmon α-phonon Fano interaction and their broadening *vs* the In content. If we artificially switch off the α and β-phonon contribution from the film conductance (*i.e.*, by removing the Lorentzian terms in Equation 2), the extinction spectra are simplified and they consist of a single absorption corresponding to the plasmon excitation. This absorption is represented in Fig. 1e (light blue solid curves). The agreement between Fano fits (panel d) and electromagnetic calculations (panel e) is very good showing the robusteness of the

main result of this paper as highlighted in Fig. 2: the 2D gas in the trivial phase constituted by massive (Schrödinger) electrons is not topologically protected, meanwhile the 2D electronic gas in the topological phase associated mainly with Dirac electrons is topologically protected from backscattering and this protection reflects in an effective reduction of the decay rate of the plasmon modes.

2 Conclusions

In this paper we have reported a study of plasmonic excitations in $(Bi_{1-x}In_x)_2Se_3$ micro-ribbon arrays by means of THz spectroscopy. We found that the plasmon behavior perfectly mirrors the single particle one, showing a sudden increase of the plasmon linewidth across the Quantum Phase Transition from the topological to a trivial insulating phase as obtained through In substitution in the Bi-site. This is a strong indication that plasmons are protected in the topological phase and this protection could open a viable path towards long quantum coherence time of plasmon states even at room temperatures, if all other plasmon decay channels can be carefully controlled and possibly reduced.

References

1 M. Z. Hasan and C. L. Kane, *Rev. Mod. Phys.* **82**, 3045–3067 (2010).

2 C. L. Kane and E. J. Mele, *Phys. Rev. Lett.* **95**, 226801 (2005).

3 J. E. Moore, *Nature* **464**, 194–198 (2010).

4 C. Niu, Y. Dai, Y. Zhu, Y. Ma, L. Yu, S. Han, and B. Huang *Scientific Reports* **2**, 976 doi:10.1038/srep00976 (2012).

5 C Niu, Y. Dai, M. Guo, W. Wei, Y. Ma, and B. Huang, *Appl. Phys. Lett.* **98**, 252502 (2011).

6 P. Di Pietro, M. Ortolani, O. Limaj, A. Di Gaspare, V. Giliberti, F. Giorgianni, M. Brahlek, N. Bansal, N. Koirala, S. Oh, P. Calvani and S. Lupi, *Nat. Nanotech.* **8**, 556-560 (2013).

7 L. Fu, *Phys. Rev. Lett.* **100**, 096407 (2008).

8 A. Kitaev and J. Preskill, *Phys. Rev. Lett.* **96**, 110404 (2006).

9 X. Zhang, J. Wang and S. C. Zhang, *Phys. Rev. B* **82**, 245107 (2010).

10 Y. L. Chen and J. G. Analytis and J.-H. Chu and Z. K. Liu and S.-K. Mo and X. L. Qi and H. J. Zhang and D. H. Lu and X. Dai and Z. Fang and S. C. Zhang and I. R. Fisher and Z. Hussain and Z.X. Shen, *Science* **325**, 178–181 (2009).

11 S A Maier, *Plasmonics: Fundamentals and Applications*, Springer (2007).

12 O. Limaj, F. Giorgianni, A. Di Gaspare, V. Giliberti, G. de Marzi, P. Roy, M. Ortolani, X. Xi, D. Cunnane and S. Lupi, *ACS Photonics* **1**, 570–575 (2014).

13 F. D'Apuzzo, P. Candeloro, F. Domenici, M. Autore, P. Di Pietro, A. Perucchi, P. Roy, S. Sennato, F. Bordi, E. M. Di Fabrizio and S. Lupi, *Plasmonics* **10**, 45–50 (2014).

14 O. Limaj, F. D'Apuzzo, A. Di Gaspare, V. Giliberti, F. Domenici, S. Sennato, F. Bordi, S. Lupi and M. Ortolani, *The Journal of Physical Chemistry* **C 117**, 19119-19126 (2013).

15 A. Toma, S. Tuccio, M. Prato, F. De Donato, A. Perucchi, P. Di Pietro, S. Marras, C. Liberale, R. Proietti Zaccaria, F. De Angelis, L. Manna, S. Lupi, E. Di Fabrizio and L. Razzari, *Nano Lett.*, **15**, 386–391 (2015).

16 F. H. L. Koppens, D. E. Chang, and F. J. Garcia de Abajo, *Nano Lett.* **11**, 3370 (2011).

17 A. N. Grigorenko, M. Polini, and K. S. Novoselov, *Nat. Photonics* **6**, 749 (2012).

18 L. Ju, B. Geng, J. Horng, C. Girit, M. Martin, Z. Hao, H. A. Bechtel, X. Liang, A. Zettl1, Y. R. Shen, and F. Wang, *Nat. Nanotech.* **6**, 630-634 (2011).

19 H. Yan, Z. Li, X. Li, W. Zhu, P. Avouris, and F. Xia, *Nano Lett.* **12**, 3766-3771 (2012).

20 I. Crassee, M. Orlita, M. Potemski, A. L. Walter, M. Ostler, Th. Seyller, I. Gaponenko, J. Chen, and A. B. Kuzmenko, *Nano Lett.* **12**, 2470-2474 (2012).

21 F. J. García de Abajo, ACS Photon.**1**,135 (2014).

22 S. Raghu, Suk Bum Chung, Xiao-Liang Qi, and Shou-Cheng Zhang, *Phys.Rev. Lett.* **104**, 116401 (2010).

23 S. J. Allen, Jr., D. C. Tsui, and R. A. Logan, *Phys.Rev. Lett.* **38**, 980 (1977).

24 M. Brahlek, N. Bansal, N. Koirala, S.-Y. Xu, M. Neupane, C. Liu, M. Z. Hasan, and S. Oh, *Phys. Rev. Lett.* **109**, 186403 (2012).

25 L. Wu, M. Brahlek, R. V. Aguilar, A. V. Stier, C. M. Morris, Y. Lubashevsky, L. S. Bilbro, N. Bansal, S. Oh, and N. P. Armitage, *Nature Phys.* **9**, 410 (2013).

26 G. Di Martino, Y. Sonnefraud, M. S. Tame, S. Kéna-Cohen, F. Dieleman, S. K. Özdemir, M. S. Kim, and S. A. Maier, *Phys.Rev. Appl.* **1**, 034004 (2014).

27 N. Bansal, Y. S. Kim, M. Brahlek, E. Edrey and S. Oh, *Phys. Rev. Lett.* **109**, 116804 (2012).

28 N. Bansal, Y. S. Kim, E. Edrey, M. Brahlek, Y. Horibe, K. Iida, M. Tanimura, G.-H. Li, T. Feng, H.-D. Lee, T. Gustafsson, E. Andrei and S. Oh, *Thin Solid Film* **520**, 224–229 (2011).

29 P. Di Pietro, F. M. Vitucci, D. Nicoletti, L. Baldassarre, P. Calvani, R. Cava, Y. S. Hor, U. Schade and S. Lupi, *Phys. Rev. B* **86**, 045439 (2012).

30 R. Valdés Aguilar, A.V. Stier, W. Liu, L. S. Bilbro, D. K. George, N. Bansal, L. Wu, J. Cerne, A. G. Markelz, S. Oh and N. P. Armitage, *Phys. Rev. Lett.* **108**, 087403 (2012).

31 M. Autore, F. D'Apuzzo, A. Di Gaspare, V. Giliberti, O. Limaj, P. Roy, M. Brahlek, N. Koirala, S. Oh, F. J. García de Abajo and S. Lupi, to be published in *Advanced Optical Materials* (2015).

32 R. E. Glover III, *et al.*, *.M. Phys. Rev.* **108**, 243 (1957).

33 M. Dressel and G. Gruener, Electrodynamics of solids, Cambridge University Press (2002).

34 V. Giannini, Y. Francescato, H. Amrania, C. C. Philips, S. A. Maier, *Nano Lett.* **11**, 2835–2840 (2011).

35 Y. Ando, *J. Phys. Soc. Jpn.* **82**, 102001–102032 (2013).

36 S. Kim, S. Yoshizawa, Y. Ishida, K. Eto, K. Segawa, Y. Ando, S. Shin, and F. Komori *Phys. Rev. Lett.* **112**, 136802–136805 (2014).

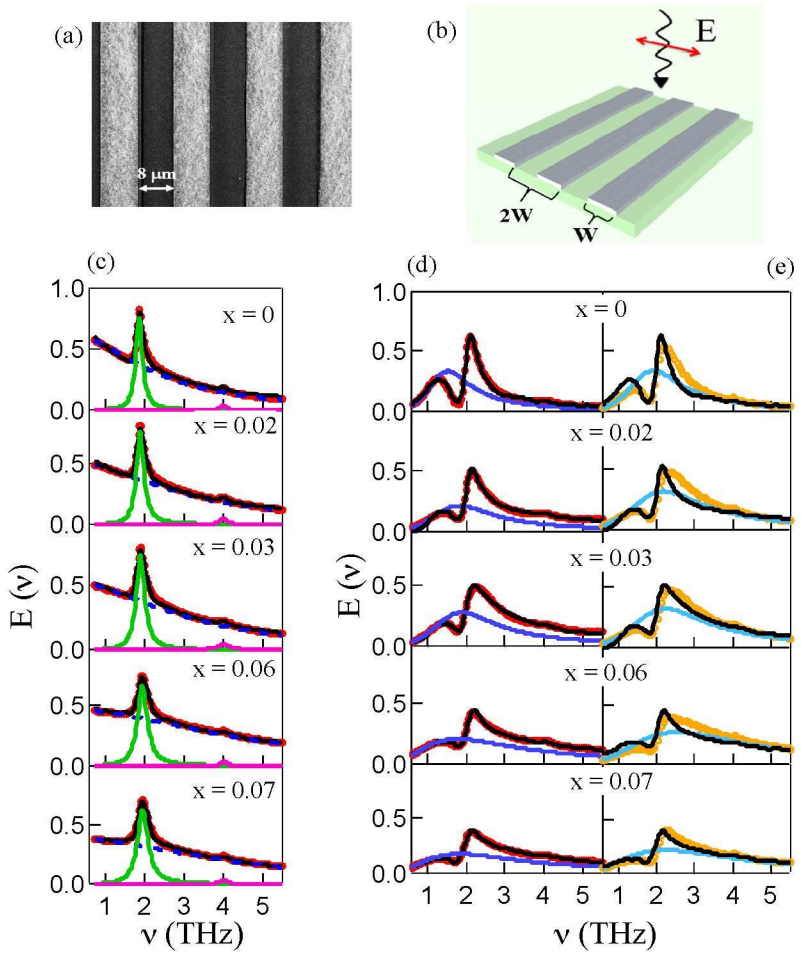

Fig. 1 (a) SEM image of the ribbon array patterned $x = 0$ film. (b) Optical scheme of the THz experiment. (c) Experimental extinction spectra at 10 K for unpatterned $(Bi_{1-x}In_x)_2Se_3$ thin films (black solid lines) fitted to Eq.1, using a Drude-Lorentz model for the conductance (red circles). The different contributions in the Drude-Lorentz fit are shown separately: Drude term (blue dashed line), α- (green) and β-phonon (purple). (d) Extinction spectra (black solid lines) for ribbon array patterned $(W = 8\mu m)$ films, with light polarization perpendicular to the ribbons. Fano fit for plasmon-phonon interaction to Eq.3 (red empty circles) at 10 K. The bare plasmon curve is represented as solid blue line. (e) Analytical calculations by means of electromagnetic simulation (orange empty circles), with bare plasmon analytical curves represented as light blue lines, obtained by artificially switching off the α phonon (see text).